Angular momentum effects in the ionization-with-excitation process of open and closed 3*d*-shell states of zinc atoms

L. Pravica,[1,2] J. F. Williams,[1,2,*] D. Cvejanović,[1,2] and S. A. Napier[1]
[1]*Centre for Atomic Molecular and Surface Physics, Physics Department, University of Western Australia, Perth 6009, Australia*
[2]*ARC Centre for Antimatter-Matter Studies, Physics Department, University of Western Australia, Perth 6009, Australia*
(Received 6 September 2006; revised manuscript received 24 November 2006; published 31 January 2007; publisher error corrected 5 February 2007)

Low-energy, polarized-electron scattering from ground state zinc atoms has explored the influence of open and closed 3*d*-shell effects in the ionization-with-excitation scattering process. Observations of nonzero values of the Stokes P_2 parameter of the 589.4 nm photons from the open-shell $3d^9 4s^2\ ^2D_{3/2}$ ionic state reveals spin-orbit interaction effects. In contrast, negligible spin-orbit interaction was deduced from the vanishing Stokes P_2 parameter of the 602.2 nm photons from the closed-shell $3d^{10}5d\ ^2D_{3/2}$ ionic state, for which the core-valence correlation is less important. A strong resonance in the closed-shell transition was observed in the P_3 parameter, about 0.8 eV above the excitation threshold with positive orientation. There are indications of a resonance in the open-shell transition.

DOI: 10.1103/PhysRevA.75.012721 PACS number(s): 34.80.Dp, 34.80.Nz, 34.80.Pa

I. INTRODUCTION

Fundamental details of atomic structure and dynamics, such as energy levels, state lifetimes, negative ion resonances, excitation functions, differential and total cross sections, and polarizations, have been obtained from collision processes using incident photons, electrons, and ions [1–3]. Recent advances [4,5] have concerned angular momentum and electron correlation effects, particularly following collaboration between experiment and theory. Here we look at disentangling angular-momentum-dependent aspects of electron-atom scattering by using spin-polarized electrons.

The fundamental aspects of spin-dependent electron scattering have been developed by Kessler [6] and Hanne [7,8] and more recently by Al-Khateeb *et al.* [9] and by Yu *et al.* [10]. In general, the interaction probability depends on electron exchange (and thus on the relative orientation of the incident and target electron spins), and also on the spin-orbit interaction, be it involving the continuum electron or within the target atom itself. The spin-dependent interactions are then naturally dependent on the initial atomic configuration. This dependence has been studied for elastic scattering [11] (and references therein) by observing spin-asymmetry functions using atomic targets with closed and open shells, namely, zinc, cadmium, and indium. A similar approach has been adapted to inelastic scattering from indium. It was observed that for elastic scattering of electrons from atoms with closed shells the spin asymmetry of the scattered electrons was caused by their spin-orbit interaction in the screened nuclear field, while for open-shell atoms it was caused by a combination of the fine-structure effect and electron exchange. In contrast, for inelastic scattering the exchange interaction was the main cause of the spin asymmetry for both open- and closed-shell atoms. Here we use incident polarized electrons to ionize and excite ground state zinc atoms into open and closed 3*d*-shell states. Integral polarizations of the photons emitted from these states are measured and this allows spin effects attributable to spin-orbit, exchange, and electron correlations to be discerned [12].

The highly correlated process of ionization with simultaneous excitation is of particular interest and it presents considerable challenges for both theoretical and experimental studies. The measurement of integrated Stokes parameters using spin-polarized electrons offers a simplified way to obtain more detailed information on the orientation and alignment of the excited ion without coincidence measurements. The transitions investigated here are chosen to highlight the spin-dependent interactions and their dependence on the location of the hole or electron state created by ionization. The investigation of the two different *d* orbitals (one excitation from the inner 3*d* orbital and other into the 5*d* orbital) illustrates properties of the 3*d* core orbital via spin-dependent scattering. Studies involving the *d* orbitals in zinc offer a unique way to probe the configuration interaction and its inter-relationship with spin-dependent forces.

The dynamical interactions between the valence and core electrons result in the polarized core less effectively screening the nuclear charge, and thus to an increase in the binding energy for the valence electrons. This core polarization potential is largely determined by the static dipole polarizability of the core. The core polarization changes the electron-electron interaction between the two valence electrons in the near-threshold region, and also the interaction between the two escaping electrons and the pair with the residual ion. Also, for configurations having electrons occupying the 3*d* single-particle state the detailed specification of the wave functions for the core electrons is dependent on the configuration of the valence electrons. As a first approximation the electron distribution of the other inner-shell electrons is insensitive to the quantum state of the valence electrons. This occurs because the 3*d* orbital intrudes more deeply into the core than any of the other valence orbitals, as seen by comparing the radial wave functions of the *nd* and 4*s* electrons.

More details of the atomic structure and scattering processes emerge from considerations of the polarization of the incident electrons and radiated photons, in particular, the spin-polarized incident electron studies [10] of ionization

*Electronic address: jfw@cyllene.uwa.edu.au

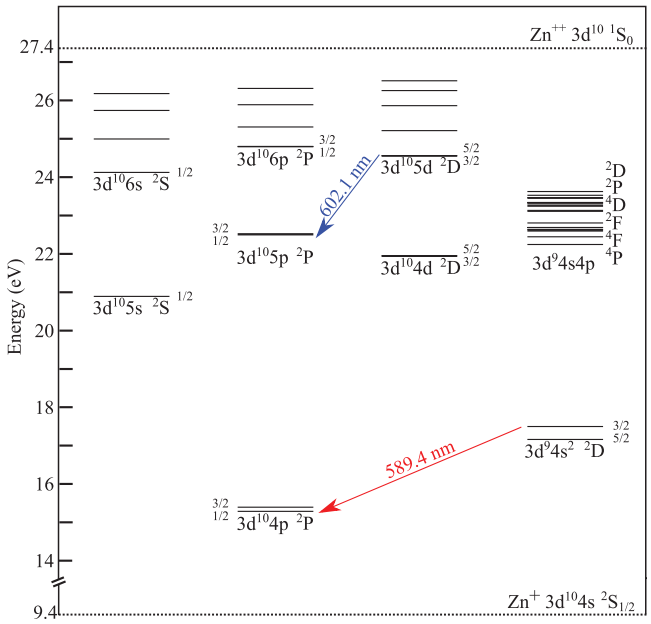

FIG. 1. (Color online) An energy level diagram for zinc ion indicating the studied transitions.

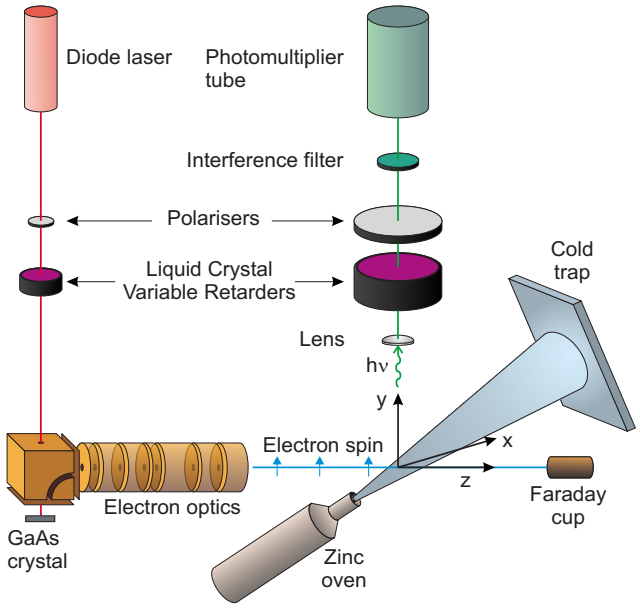

FIG. 2. (Color online) A schematic diagram of the experiment.

with excitation from the ground $3d^{10}4s^2\ ^1S_0$ atomic state to the excited $3d^94s^2\ ^2D_{3/2}$ open $3d$-shell state of the zinc ion which decays to the $3d^{10}4p\ ^2P_{1/2}$ state by emission of a 589.4 nm photon. This study illustrates the physical importance and interpretation of the observed integrated Stokes parameters (i.e., integrated over all the scattering angles of the undetected scattered electrons) and how they relate to electron exchange and the spin-orbit interaction [12]. The only other measurements of polarization of emitted light from the decay of the $3d^94s^2\ ^2D_{3/2}$ ion states that we know of used unpolarized electrons [13] or photon impact [14].

Extending the idea of a comparative study of an open and closed shell [11] we chose two transitions with an open and closed $3d$ shell in zinc to also highlight the specifics of the $3d$ core orbital and show how, and to what extent, the polarization of emitted light can be used to test the fine effects associated with the spin-orbit interaction and configuration mixing. In addition to the studies of $3d^94s^2\ ^2D_{3/2}$ we studied a second $^2D_{3/2}$ to $^2P_{1/2}$ transition; the closed $3d$-shell $3d^{10}5d\ ^2D_{3/2}$ ionic state which decays by emitting 602.2 nm radiation. Both transitions are indicated in Fig. 1. Although the two studied transitions connect the states with different electronic configurations the overall symmetries are the same.

In a previous study of the $3d^94s^2\ ^2D_{3/2}$ state, Yu *et al.* [10] showed, within about 4 eV of threshold, that the spin-orbit interaction was negligibly small compared to the experimental uncertainties, so *LS* coupling seemed to apply. The residual ion was found to be both aligned and oriented. Also, negative angular momentum transfer occurred, as evidenced by the appropriate Δm_j change and the combination of electron exchange and fine-structure coupling. However, the extent of the coupling between the $3d$ shell and the $4s$ and $4p$ electrons, the electron configuration interaction effects, and the resonance effects were not accessible from this single study. Also Yu *et al.* [10] used previously misprinted values [14] for the nuclear abundances in their calculations of the integrated state multipoles. The correct nuclear abundances for zinc (95.9% and 4.1% for the nuclear spins $I=0$ and 5/2, respectively) have to be used to correct their values. For those reasons we reconsider this investigation and present the corrected, and statistically significantly improved, integrated state multipoles for $3d^94s^2\ ^2D_{3/2}$ excitation. The present study illustrates how small effects can be observed and different conclusions made when accuracy in polarization measurements is improved.

In Sec. II we describe our approach for integral polarization measurements using incident spin-polarized electrons. In Sec. III we report our observations of the three integrated Stokes parameters for the open $3d$-shell (589.4 nm) and closed $3d$-shell (602.2 nm) transitions and discuss the integrated state multipoles.

II. THE EXPERIMENTAL APPROACH

The apparatus and experimental geometry are shown in Fig. 2. In the rectangular coordinate system (x,y,z) the incident electron momentum vector defines the z axis, and the electron polarization defines the y axis. Photons are detected along the y axis and from the observed intensities $I(\beta)$ we determine the Stokes parameters (as defined in [16]) as $P_1=[I(0°)-I(90°)]/[I(0°)+I(90°)]$, $P_2=[I(45°)-I(135°)]/[I(45°)+I(135°)]$, and $P_3=[I(\sigma^-)-I(\sigma^+)]/[I(\sigma^-)+I(\sigma^+)]$. Here $I(\beta)$ is the intensity of photons with a polarization angle β with respect to the z axis, and $I(\sigma^+)$ and $I(\sigma^-)$ are, respectively, the intensities of photons with positive and negative helicity. We do not observe the scattered electrons, so the Stokes parameters are integrated over all scattering angles. The advantage of using spin-polarized electrons for integral polarization measurements is that a larger number of

parameters can be measured, giving greater insight into the scattering process. The method yields much higher counting rates than photon-electron coincidence measurements, and hence allows the study of weaker transitions.

For unpolarized electron impact only the integrated P_1 parameter will be nonzero since only the z-axial symmetry is defined for the collision process [17]. However, transversely polarized electrons (spin along the y axis) result in an excitation process with planar symmetry with respect to reflection in the xz plane, and hence P_2 and P_3 may also be nonzero. P_2 will be nonzero if there is a significant spin-orbit interaction, while P_3 can be caused by the electron exchange and/or the spin-orbit interaction [12]. Hence observation of the integrated Stokes parameters P_2 and P_3 allows disentanglement of the spin-dependent interactions from the usually much stronger Coulomb interaction.

The Stokes parameters can be related to the alignment and orientation of the excited state by state multipoles which are linear combinations of the excited-state density matrix elements. The definition of the state multipoles and their relation to the Stokes parameters is given, for example, by Blum [26]. After integration over all scattering angles and normalization to the cross section $\langle \mathcal{T}^+_{00}(J)\rangle$ only three parameters are necessary to parametrize the integrated Stokes parameters [12] $\langle \mathcal{T}^+_{20}(J)\rangle$ obtainable by unpolarized electrons, and $\langle \mathcal{T}^+_{11}(J)\rangle$ and $\langle \mathcal{T}^+_{21}(J)\rangle$ which can be obtained only from experiments with transversely polarized electrons. They are related to the two alignment parameters and the orientation of the excited state, respectively.

By normalizing the state multipoles to the corresponding zero-rank multipoles, the normalized electric quadrupole moments $T^+_{20}(J), T^+_{21}(J)$ and the normalized magnetic dipole moment $T^+_{11}(J)$ for the total angular momenta can be determined using

$$T_{20}(J) \equiv \frac{\langle \mathcal{T}^+_{20}(J)\rangle}{\langle \mathcal{T}_{00}(J)\rangle} = \frac{4.167P_1}{1.009P_1 - 3.027}, \tag{1}$$

$$T_{21}(J) \equiv \frac{\langle \mathcal{T}^+_{21}(J)\rangle}{\langle \mathcal{T}_{00}(J)\rangle} = \frac{-2.552P_2}{1.009P_1 - 3.027}, \tag{2}$$

$$T_{11}(J) \equiv \frac{\langle \mathcal{T}^+_{11}(J)\rangle}{\langle \mathcal{T}_{00}(J)\rangle} = \frac{1.962P_3}{1.009P_1 - 3.027}. \tag{3}$$

Furthermore, if LS coupling holds, the normalized electric quadrupole moment $T^+_{20}(L)$ of the orbital angular momentum and the normalized magnetic dipole moment $T^+_{11}(S)$ for the spin angular momentum can be determined as

$$T_{20}(L) \equiv \frac{\langle \mathcal{T}^+_{20}(L)\rangle}{\langle \mathcal{T}_{00}(L)\rangle} = \frac{4.980P_1}{1.009P_1 - 3.027}, \tag{4}$$

$$T_{11}(S) \equiv \frac{\langle \mathcal{T}^+_{11}(S)\rangle}{\langle \mathcal{T}_{00}(S)\rangle} = \frac{9.813P_3}{7.061P_1 + 6.768}. \tag{5}$$

The apparatus shown in Fig. 2 is similar in principle to that used previously in our laboratory [15]; however, this apparatus incorporates some important new features. The two main parts of the apparatus, the sources of the spin-polarized electrons and zinc atoms, are located in separate vacuum chambers with pressures of 10^{-10} and 10^{-8} Torr, respectively, connected via a 1 mm circular aperture which can be closed by a thin valve [18]. Polarized electrons were emitted from a GaAs crystal surface [15] after photoexcitation by circularly polarized laser light with a wavelength of 830 nm. A strained GaAs crystal can provide an electron spin polarization up to 75%. The angular momentum of the circularly polarized laser photons was transferred to the spin-orbit-split $^2P_{3/2}$ and $^2P_{1/2}$ states of the crystal which were selectively populated. The preparation of the crystal surface by cesium and oxygen deposition gave it negative electron affinity and enabled the extraction of the electrons with polarization perpendicular to the surface. Electric fields were used to extract, accelerate, and deflect the electron beam by 90° so that electrons entered the scattering region with the spin vector transverse to the linear momentum vector and along the positive y axis.

All of the electron optics used to transport and focus the electron beam is situated in ultrahigh vacuum and protected from zinc vapor. The electrons were focused into the collision chamber where they collided with zinc atoms in their ground state. Zinc atoms were produced by a resistively heated metal vapor oven. The oven was designed specifically to overcome the main problems associated with this type of experiment, for example, heat and light radiation from hot elements and stray electric and magnetic fields. The focusing of the electron beam was achieved by measuring and optimizing the ratio of electron currents through two circular apertures which created central and annular beam collectors of a Faraday cup.

The polarization of the photons was analyzed by a linear polarizer and a liquid crystal variable retarder [19]. A particular atomic state was selected by filtering the wavelength of photons by an interference filter. The interference filters were 589.4 and 602.2 nm with 0.6 and 1 nm full width at half maximum, respectively. The observations of the 589.4 and 602.2 nm photons were limited to several eV above each threshold (17.51 and 24.02 eV, respectively) to limit the effects of cascades. Energy separation between neighboring states was sufficient to isolate observed state-specific photons. Photons were detected by a photomultiplier tube followed by a preamplifier, discriminator, and NIM-to-TTL converter (NIM denotes nuclear instrumentation modules, TTL denotes transistor-transistor logic). The experiment was controlled and data recorded via a data acquisition card on a computer.

Additionally to the above mentioned correction of polarization for isotope effects, the present data were corrected for depolarization due to the residual magnetic field. This was especially prominent for the long-lived $3d^9 4s^2\ ^2D_{3/2}$ open-shell state (1870 ns) for which the depolarization due to a residual magnetic field of 5 mG amounts to approximately 1.7%.

The polarization of the electron beam was measured via the integrated Stokes parameter P_3 for the $5s\ ^3S_1$ to $4p\ ^3P_2$ transition [20] of the neutral atom. Any optical effect related to the spin appears only through the spin-orbit interaction. This interaction must be strong enough to allow the fine

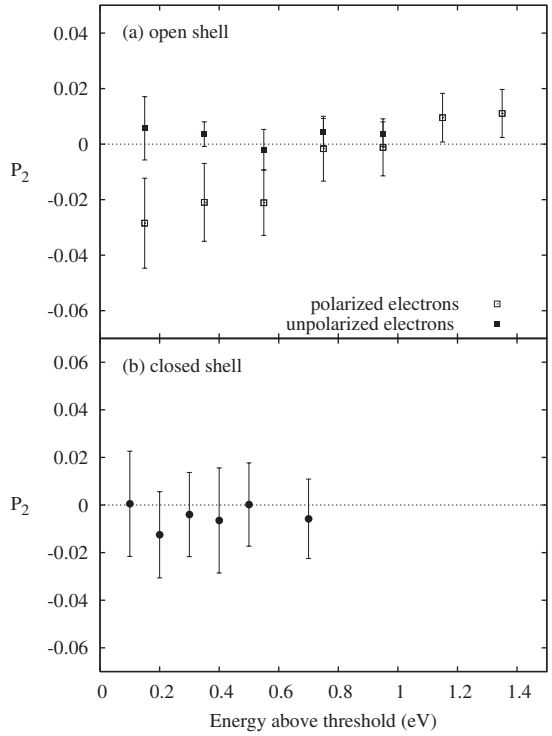

FIG. 3. Integrated Stokes parameter P_2 for the (a) $3d^9 4s^2\ ^2D_{3/2}$ open- and (b) $3d^{10}5d\ ^2D_{3/2}$ closed-shell states with 589.4 and 602.2 nm wavelengths, respectively.

splitting of the atomic ^3P_J levels to be resolved in optical measurements, but not so large as to lead to a breakdown of *LS* coupling. For the measured final $J=2$ state the theory predicts [20] that the circular polarization should be half of the incident electron polarization at the cascade-free region near threshold, which was also observed. The presented Stokes parameters have been normalized using the measured values of the incident electron beam polarization of 66%.

III. RESULTS AND DISCUSSION

The measurements of P_1, P_2, and P_3 for the $3d^9 4s^2\ ^2D_{3/2}$ and $3d^{10}5d\ ^2D_{3/2}$ states are shown in Figs. 3–5. The normalized state multipoles, shown in Figs. 6 and 7, are also presented here to aid the discussion.

The most difficult aspect of the Stokes parameter measurements was obtaining adequate statistics for P_2. $I(45°)$ and $I(135°)$ were both small quantities and their difference was small. Thus a high level of accuracy was required before P_2 could be determined confidently as zero or nonzero. The P_2 data in Fig. 3(a) were obtained using a 66% polarized electron beam for increased sensitivity. This figure shows small nonzero values of P_2 for the $3d^9 4s^2\ ^2D_{3/2}$ state in the first 0.6 eV above threshold. Previous results [10] using electrons with 30% polarization showed smaller values with larger uncertainties of 0.01 ± 0.06 so that they were interpreted as zero. Considerable effort has been made with these additional measurements to reduce the size of the error bars.

To verify this nonzero P_2 measurement the experiment was repeated using unpolarized electrons, for which a zero value of P_2 is expected. The average value over the five data points is 0.003 ± 0.012 which we accept as the zero value for the apparatus at that time, in that mode of operation.

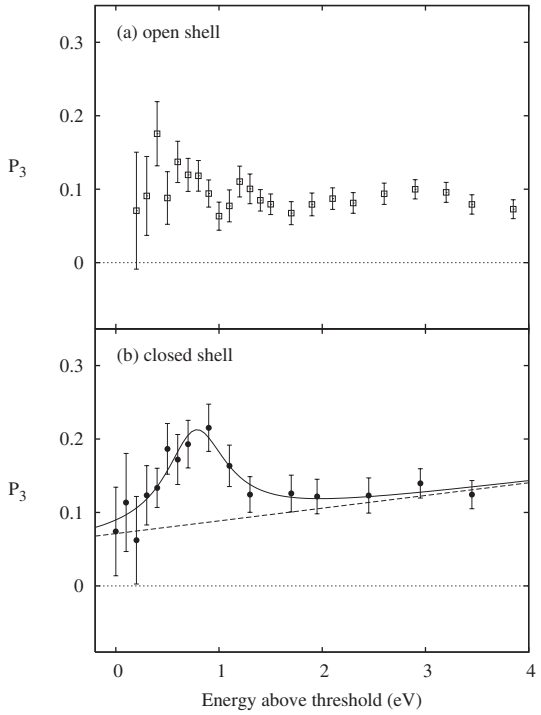

FIG. 4. Integrated Stokes parameter P_3 for the (a) $3d^9 4s^2\ ^2D_{3/2}$ open- and (b) $3d^{10}5d\ ^2D_{3/2}$ closed-shell states with 589.4 and 602.2 nm wavelengths, respectively. For (b) the full line shows the fitted Fano profile and the dashed line shows the background contribution to the polarization.

The measured values of P_2 for the closed-shell 602.2 nm transition are shown in Fig. 3(b). For this transition the average value of P_2 was -0.007 ± 0.019 which we interpret as indicating no observable spin-orbit interaction. We conclude then that the nonzero value of P_2 for the 589.4 nm transition indicates the violation of *LS* coupling as a consequence of the opening, and hence polarization, of the $3d$ shell.

Andersen and Bartschat [17] point out that a combination of spin-orbit interaction and configuration mixing makes it

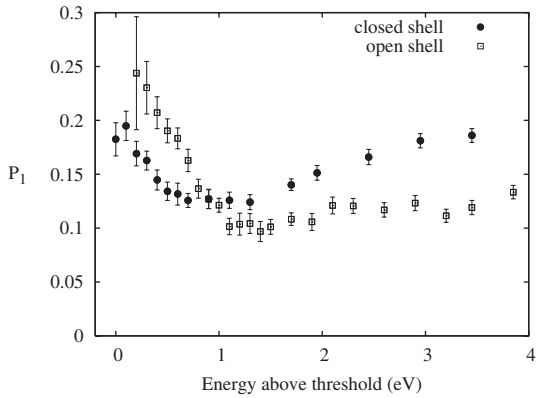

FIG. 5. Integrated Stokes parameter P_1 for the $3d^9 4s^2\ ^2D_{3/2}$ open- and $3d^{10}5d\ ^2D_{3/2}$ closed-shell states with 589.4 and 602.2 nm wavelengths, respectively.

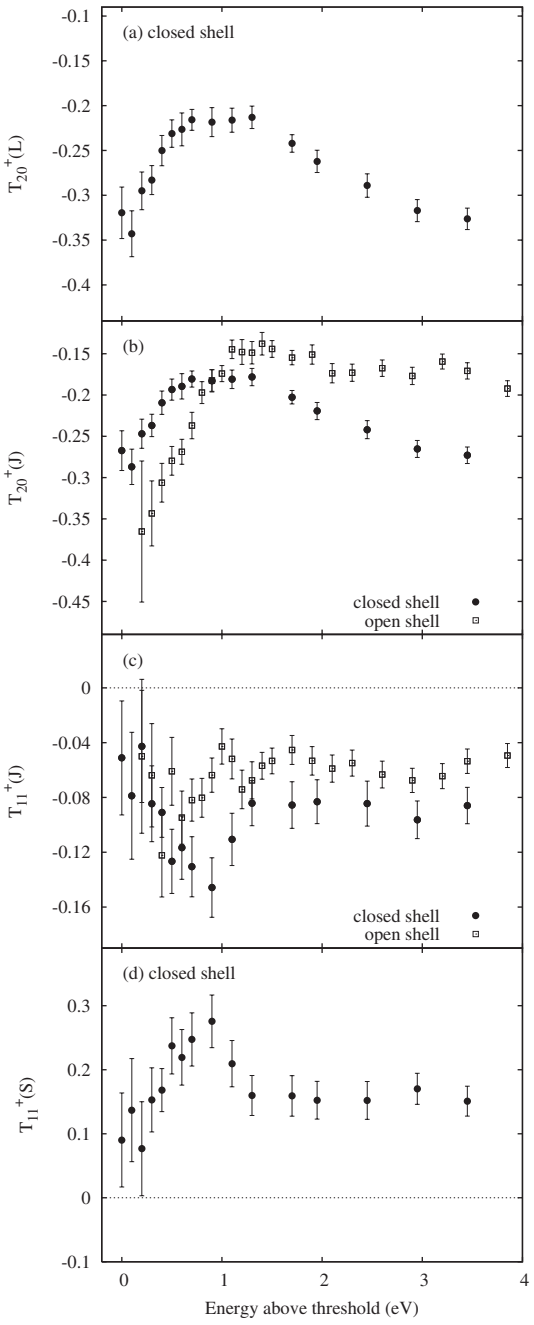

FIG. 6. Normalized state multipole moments for the $3d^9 4s^2\ ^2D_{3/2}$ open- and $3d^{10}5d\ ^2D_{3/2}$ closed-shell states with 589.4 and 602.2 nm wavelengths, respectively. (a) Electric quadrupole moment of the orbital angular momentum $T^+_{20}(L)$; (b) electric quadrupole moment of the total angular momentum $T^+_{20}(J)$; (c) magnetic dipole moment of the total angular momentum $T^+_{11}(J)$; (d) magnetic dipole moment of the spin angular momentum $T^+_{11}(S)$.

impossible to describe the excitation using *LS* coupling. A naive analysis might conclude that, since both transitions are from $^2D_{3/2}$ states, the photon polarization properties will be similar. However, their total angular momenta are derived from different configurations, a hole in the $3d$ orbital (an unpaired $3d$ electron) for the open-shell transition and an electron in the higher-energy $5d$ orbital outside a fully occupied $3d$ shell for the closed-shell transition. We interpret then

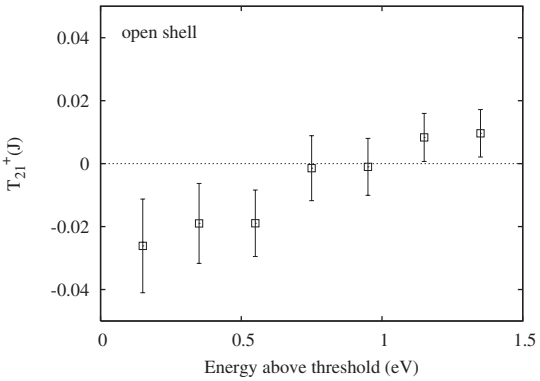

FIG. 7. Normalized electric quadrupole moment $T^+_{21}(J)$ of the total angular momentum for the $3d^9 4s^2\ ^2D_{3/2}$ open-shell state with 589.4 nm wavelength.

the nonzero values of P_2 for the open-shell transition as being a consequence of configuration mixing in the $3d$ orbital of Zn combined with spin-orbit interaction. Theoretical interpretations of zinc ejected electron spectra [21] and the description of corresponding autoionizing states associated with $3d$ electron ejection by Mansfield [22] have demonstrated this configuration mixing. Also, the modeling of photoionization [23,24] reveals the role of spin-orbit effects and inner-core shielding for the $3d$ electrons [24]. For example, the study of photoionization of neutral zinc using the multiconfiguration relativistic random-phase approximation theory by Wang *et al.* [24] indicated that angular distribution and spin-polarization parameters all show strong dependence on core shielding effects which are primarily due to excitation of the $3d$ electrons. These parameters, and also the Stokes parameters reported here, are sensitive to the interplay between correlation and relativistic effects, and so provide both an important set of data for comparison and also a stringent test of theory.

The experimental data for the circular polarization P_3, are shown in Figs. 4(a) and 4(b). The energy behavior for the closed-shell transition is dominated in the near-threshold region by what seems like a resonance, and there is also an indication of possible resonance contributions in the open-shell transition. Considering the present energy resolution of 0.25 eV the observed structures may be a mixture of more than one unresolved resonance state. Nevertheless the structure in the closed-shell transition was fitted to a Fano profile in the usual way [25] to indicate its width of 0.71 ± 0.22 eV and an energy of 24.76 ± 0.34 eV. The data indicate also that the resonance in the 602.2 nm transition has a positive value of P_3. These will be studied further when spin-polarized electrons are produced with better resolution.

The measurements of P_3 for the open- and closed-shell transitions at the threshold gave similar values, but with large experimental uncertainties. The data show nonzero values indicating that the residual ion is oriented by the angular momentum transfer between the incident electron and the target atom. Generally this can occur through electron exchange and/or spin-orbit interaction [12]. For the closed-shell transition, zero values of P_2 indicate that the spin-orbit interaction is negligible. Hence the transfer of angular mo-

mentum from the incoming electron occurs only through electron exchange followed by a transfer of spin into orbital angular momentum via fine-structure interaction. For the open-shell transition small but nonzero values of P_2 are sign of violation of the *LS* coupling. However, the dominant process is still exchange followed by fine-structure interaction as indicated by the similar values and signs of P_3 for the two transitions.

The Stokes parameter P_1 for the decay photons from the open- and closed-shell transitions is shown in Fig. 5. The nonzero values of P_1 imply that the residual ion is aligned along the direction of the propagation of the initial electron beam. The energy dependence of P_1 for the two transitions is somewhat different. P_1 for the open-shell transition is higher at threshold, but decreases more sharply, and falls below the closed-shell P_1 value approximately 0.8 eV above threshold. Above this energy the open-shell P_1 remains steady, while the closed-shell P_1 increases. The present values of P_1 for the open-shell transition are in good agreement with earlier measurements by Hipp *et al.* [13] within similar uncertainties. Their data are not shown here for clarity.

The analysis of the data using state multipoles can, in some cases, reveal information additional to the Stokes parameters. For example, the state multipoles for the well *LS*-coupled closed-shell $3d^{10}5d\ ^2D_{3/2}$ state allow the total and spin angular momentum transfers to be separated and hence the electric quadrupole moment of the orbital angular momentum Fig. 6(a) and the magnetic dipole moment of the spin angular momentum Fig. 6(d) to be obtained. This information complements the electric quadrupole Fig. 6(b) and magnetic dipole Fig. 6(c) moments of the total angular momenta which can be obtained even for non-*LS*-coupled states such as the closed-shell $3d^94s^2$ state. The significance of the separation of the spin and orbital momentum transfers is described below.

For the closed-shell transition, the electric quadrupole moments for the orbital and total angular momenta shown in Figs. 6(a) and 6(b) indicate similar energy dependencies. However, the magnitude of the quadrupole moment for the total angular momentum is reduced relative to the moment for the orbital angular momentum, due to the fine-structure coupling.

Figures 6(c) and 6(d) show that for the closed-shell transition the magnetic dipole moment for the total angular momentum is reduced relative to the spin angular momentum, and that it also changes sign. The positive value of the spin magnetic dipole indicates positive angular momentum transfer from the incident electron via electron exchange. However, the negative value of the total magnetic dipole indicates that negative angular momentum is transferred to the residual ion when the spin couples to the orbital angular momentum, i.e., the $m=-1$ states are populated rather then the $m=+1$ states.

The angular momentum transfer along the y direction is directly proportional to the normalized state multipole $T_{11}^+(J)$ [26] since

$$\langle J_y(J)\rangle = \sqrt{\frac{2J(J+1)}{3}}T_{11}^+(J). \tag{6}$$

Figures 6(c) and 6(d) show that fine-structure coupling causes negative angular momentum transfer for this particular case of a well *LS*-coupled system in which spin-orbit interactions for both the continuum electrons and the internal electrons can be neglected.

For the open-shell process the spin-orbit interaction is not negligible as indicated by nonzero values of $T_{21}^+(J)$ in Fig. 7. This is clearly an effect of the open $3d$ shell in the ion and evidence that the outer $4s^2$ electrons do not shield the polarized core completely. The effect is very small as values of $T_{21}^+(J)$ are about 0.02 within 0.6 eV from the threshold.

For the open-shell transition the spin and the orbital parts cannot be separated because of the spin-orbit interaction. However, comparing the open- and closed-shell state multipoles is still instructive. Figures 6(b) and 6(c) show both transitions exhibiting very similar behavior. Close to the threshold, the open-shell process shows slightly higher $T_{20}^+(J)$ while the uncertainties of the measurements do not allow such comparison for $T_{11}^+(J)$.

IV. CONCLUSION

The ionization-with-excitation process from the ground $3d^{10}4s^2$ state is a well-correlated many-body process and we investigated two different examples. For the $3d^{10}5d$ state, one $4s$ electron has been ejected and the other excited to the $5d$ state outside a closed $3d$ orbital. In contrast, for the $3d^94s^2$ state, one $3d$ electron has been ejected and the two $4s$ electrons are screening the $3d$ hole while two electrons, scattered and ejected, are escaping. This obviously complex rearrangement accompanied with near-threshold excitation regime where electron correlations (including the scattered and ejected electrons) are important, has provided an insight into the role of spin-orbit interaction within the $3d$ atomic core orbital, as compared to the $5d$ orbital located outside the valence electron region and outside a closed $3d$ core.

The measurements show how an open shell in the ionization-with-excitation process caused a breakdown of *LS* coupling while a closed-shell process remains well *LS* coupled. Furthermore, in both processes the residual ions were not only aligned but also oriented. Possible resonances in the closed shell were identified with positive values of the orientation parameter. The analysis using normalized state multipoles for the closed shell transition revealed that fine-structure coupling not only depolarized the electric quadrupole moment and the magnetic dipole moment but also changed the sign of the angular momentum transfer. Similar effects can be expected in the open-shell ion; however, the observed values may be affected by a small violation of the *LS* coupling. Further studies using photon-electron coincidence techniques are well justified to continue the exploration of the extent of these apparently ubiquitous effects of the spin-orbit interaction.

ACKNOWLEDGMENTS

This work was supported by the Australian Research Council. The expert technical assistance in design and construction by the mechanical workshop of the School of Physics made this work possible.

[1] H. S. W. Massey, E. H. S. Burhop, and H. B. Gilbody, 2nd ed. *Electronic and Ionic Impact Phenomena* (Clarendon, Oxford, 1969).
[2] E. W. McDaniel, *Atomic Collisions: Electron and Photon Projectiles* (Wiley-Interscience, New York, 1989).
[3] B. H. Bransden and C. J. Joachain, *Physics of Atoms and Molecules*, 2nd ed. (Longman, London, 2003).
[4] H. Farrokhpour, M. Alagia, M. Y. Amusia, L. Avaldi, L. V. Chernysheva, M. Coreno, M. de Simone, R. Richter, S. Stranges, and M. Tabrizchi, J. Phys. B **39**, 765 (2006).
[5] C. Herting, G. F. Hanne, K. Bartschat, K. Muktavat, R. Srivastava, and A. D. Stauffer, J. Phys. B **36**, 3877 (2003).
[6] J. Kessler, *Polarized Electrons* (Springer-Verlag, Berlin, 1976).
[7] G. F. Hanne, Phys. Rep. **95**, 95 (1983).
[8] G. F. Hanne, *Coherence in Atomic Collision Physics* (Plenum Press, New York, 1988), Chap. 2, pp. 41–88.
[9] H. M. Al-Khateeb, B. G. Birdsey, and T. J. Gay, Phys. Rev. Lett. **85**, 4040 (2000).
[10] D. H. Yu, L. Pravica, J. F. Williams, N. Warrington, and P. A. Hayes, J. Phys. B **34**, 3899 (2001).
[11] M. Bartsch, H. Geesmann, G. F. Hanne, and J. Kessler, J. Phys. B **25**, 1511 (1992).
[12] K. Bartschat and K. Blum, Z. Phys. A **304**, 85 (1982).
[13] M. Hipp, P. Bopp, A. Gotz, and W. Mehlhorn, J. Phys. B **24**, L453 (1991).
[14] W. Kronast, R. Huster, and W. Mehlhorn, Z. Phys. D: At., Mol. Clusters **2**, 285 (1986).
[15] P. A. Hayes, D. H. Yu, and J. F. Williams, Rev. Sci. Instrum. **68**, 1708 (1997).
[16] K. Bartschat, K. Blum, G. F. Hanne, and J. Kessler, J. Phys. B **14**, 3761 (1981).
[17] N. Andersen and K. Bartschat, *Polarization, Alignment, and Orientation in Atomic Collisions* (Springer-Verlag, New York, 2001).
[18] L. Pravica, D. Cvejanovic, J. F. Williams, S. A. Napier, S. N. Samarin, and A. D. Sergeant, Rev. Sci. Instrum. **77**, 076104 (2006).
[19] J. E. Furst, D. H. Yu, P. A. Hayes, C. M. D'Souza, and J. F. Williams, Rev. Sci. Instrum. **67**, 3818 (1996).
[20] M. Eminyan and G. Lampel, Phys. Rev. Lett. **45**, 1171 (1980).
[21] C. G. Back, M. D. White, V. Pejčev, and K. J. Ross, J. Phys. B **14**, 1497 (1981).
[22] M. W. D. Mansfield, J. Phys. B **14**, 2781 (1981).
[23] K. Bartschat, J. Phys. B **20**, 5023 (1987).
[24] L. R. Wang, H. C. Chi, and K. N. Huang, Phys. Rev. Lett. **83**, 702 (1999).
[25] U. Fano, Phys. Rev. **124**, 1866 (1961).
[26] K. Blum, *Density Matrix Theory and Applications* (Plenum Press, New York, 1981).